5. PARTICIPATION IN THE TJ-II PROGRAMME[1]

C. Varandas and M.E. Manso (Heads), I. Nedzelskij, B. Gonçalves, L.A. Pereira

5.1. INTRODUCTION

The Portuguese participation in the TJ-II programme has been mainly focussed on the following areas:

- Microwave reflectometry;
- Heavy ion beam diagnostic;
- Edge plasma physics.

5.2. MICROWAVE REFLECTOMETRY

The following activity was performed in 2002:

- Beginning of the development of an heterodyne Q-band fixed frequency channel using synthesizer sources, to study radial correlation parameters of plasma turbulence.

5.3. HEAVY ION BEAM DIAGNOSTIC

5.3.1. Main activities

The following main tasks were carried out in 2002:

- Test of the trans-impedance amplifiers and development of new pre-amplifiers for the detected signals;
- Installation of the multiple cell array detector (MCAD), the manipulator system and the trans-impedance amplifiers on TJ-II;
- Development of new deep Faraday cup type cells aiming at decreasing the plasma loading effect on the measurements;
- Development of an upgrade version of the dedicate control and data acquisition software and its installation in the TJ-II system.

5.3.2. Multiple cell array detector

The first version of the MCAD (presently installed) is based on 175×400 mm Teflon printed circuit board with the edge connector for 120 (6×20) cells of 12×8 mm each. A biased stainless steel mask is placed in front of the cells at 3 mm distance. This sandwich of MCAD and biased mask is installed inside a shield box kept at earth potential (Figure 5.1). The high-vacuum and high temperature EDAC 800 series multi-pin connector performs the slide contacts with the cells. For the simultaneous measurements of the plasma potential and density fluctuations, the insertion of holes in the MCAD is foreseen for the free penetration of the secondary ions into the energy analyzer.

The first test carried out with plasma revealed a strong noise on the collected signals, produced by photoemission of the copper cells due to strong plasma loading. Using helium puffing in the end of the discharge and sweeping the primary beam, it was possible to detect the primary and secondary beams in the multiple cell array detector (Figure 5.2).

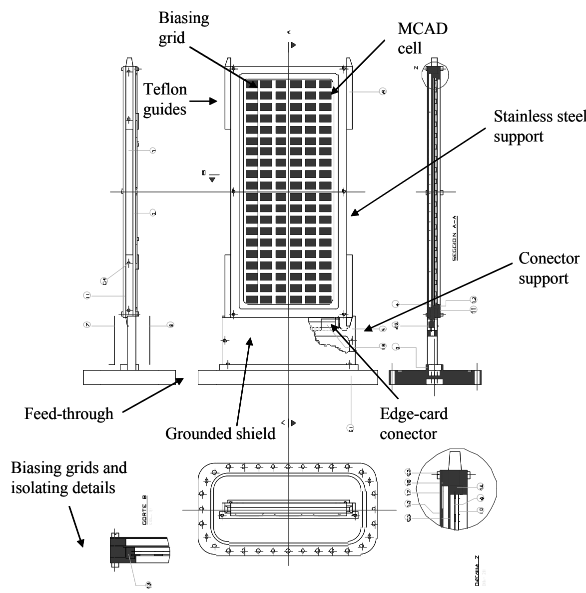

Figure 5.1 - The multiple cell array detector and the multi-pin connector. The multi-pin is enclosed on a grounded stainless steel to prevent plasma loading.

To avoid the noise due to plasma loading a new deep Faraday Cup type cell (Figure 5.3) was projected and installed. The detector consists on a copper block, inserted on a Teflon box and a stainless steel shell.

The stainless steel shell is connected to ground by welding to the exterior grid (two of the channels that go to the connector allows grid biasing) (Figure 5.4). The whole block measures 14×10 mm and has 5×8 holes. It is expected that the photoelectrons will be immediately collected by the nearest inner surface inside the hole. To

[1] Work carried out in collaboration with the TJ-II Team of the Association EURATOM/CIEMAT. Contact Persons: J. Sanchez and C. Hidalgo.

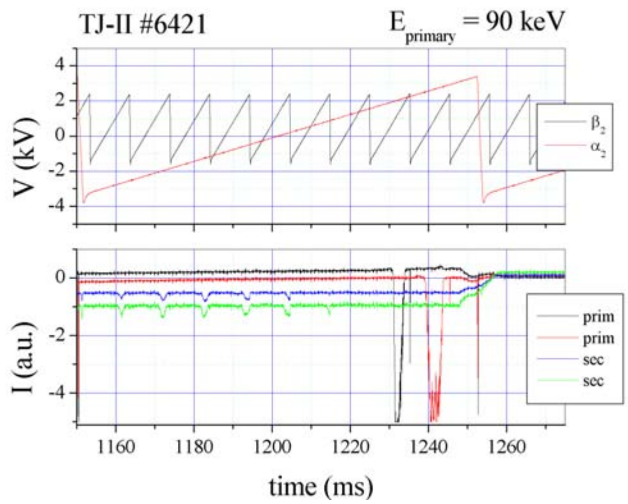

Figure 5.2 - Signals from four cells of the multiple cell array detector. Primary and secondary beams were detected

avoid damage of the cells of the Teflon support, the electric contact of the new cell with the flat copper cell is made through a clip of copper foil (Figure 5.3) which has some elasticity and provides a reliable electrical connection. It was fixed not only by compression between the copper block and the Teflon shell, but also with a drop of silver paint.

5.3.3. Control and data acquisition system

The dedicated control and data acquisition system of this diagnostic is composed by a VME system and two Personal Computers, connected by a 10 Mbit ethernet.

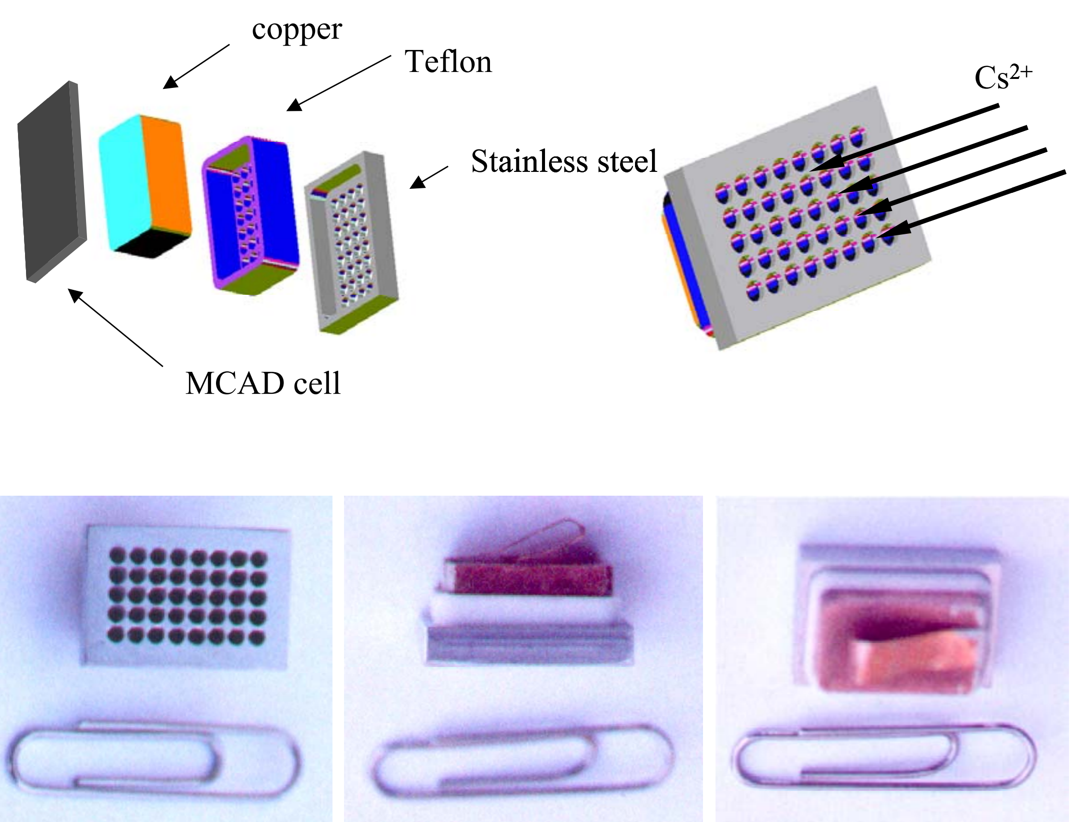

Figure 5.3 - The new deep Faraday cup type cells. This design aims at preventing the effects of plasma loading on the MCAD cells, which is mostly due to photo-electrons. It is expected that when emitted inside the holes the probability of re-absorption of the photo-electron increases.

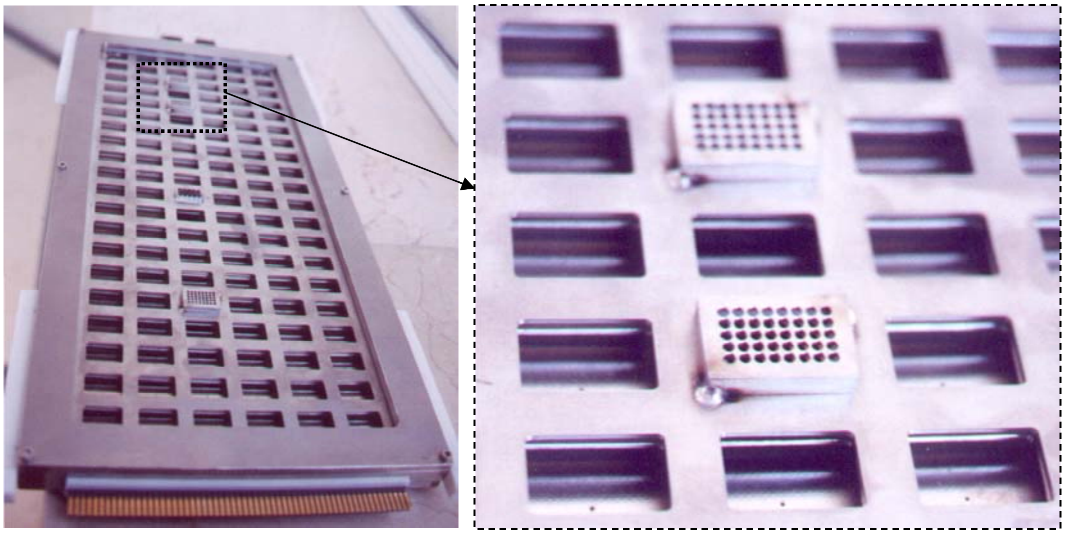

Figure 5.4 - The new deep Faraday cup cells on the MCAD

The VME system includes:

(i) A Power PC 68040 processor, with 64 MB RAM, and 10 GB IDE hard disk;

(ii) Two IST/CFN arbitrary waveform generator boards (VME 80) with the following characteristics:

- 8 independent 12-bit channels;
- 8 kWords FIFO memory;
- 1 μs of update rate;
- Signal reconstruction filter software/hardware programmable;
- Delay timer of 32 bits with 1 μs resolution (software programmable);
- 2 trigger sources, software and hardware (TTL positive edge from VME P2 connector);
- Bipolar/unipolar output, jumper selectable;
- Bipolar output voltage range of ±2.5 V, ±5 V or ±10 V, jumper selectable;
- Unipolar output voltage range of 0-5 V or 0-10 V, jumper selectable;
- Maximum output current of ±25 mA;
- Empty memory flag or empty memory interruption available;
- External analogue output connection through a LEMO connector;

(iii) Three CFN/IST transient recorder modules (VME 8i125) with the following characteristics:

- 8 independent, non-multiplexed acquisition channels of 12 bit resolution;
- Programmable delay and sample rate for each couple of channels with 1 μs timing resolution;
- Differential inputs, 2.5 V, over-voltage protected;
- External clock input;
- 60 dB CMRR differential inputs.

The PCs run Windows 95 and the VME controller runs the OS-9 real-time operating system as well as two daemons respectively for the VME 80 and VME 8i125 boards (Figure 5.5). Graphical client interfaces written in LabVIEW for the PCs were developed allowing to set-up the operation parameters and configurations as well as to collect the acquired data and to insert it in the TJ-II database.

5.4. EDGE PLASMA PHYSICS

5.4.1. Statistical properties of the radial correlation of turbulence in the TJ-II boundary region

This section reports the studies on the statistical properties of plasma fluctuations and turbulent transport, varying the magnetic well in the TJ-II plasma edge region. The absence of a magnetic well (i.e. magnetic hill) gives rise, in our case, to instabilities at any plasma pressure. With this in mind, a sequence of configurations has been selected with well depth ranging from 2.4 down to 0.2%, and having a magnetic well in the bulk and a magnetic hill at the plasma edge, which becomes unstable. Remarkable similarity exists among those configurations according to their rotational transform profiles as well as to their magnetic surface shapes. Experiments were carried out in ECRH plasmas, using one or gyrotrons of the TJ-II heating system (P_{ECRH} = 300 – 600 kW). A fast reciprocating Langmuir probe has been used to investigate the structure of the plasma profiles and their fluctuations. Fluctuations in the ion saturation current, floating potential and ExB turbulent flux, together with their degree of intermittence, have been observed to increase

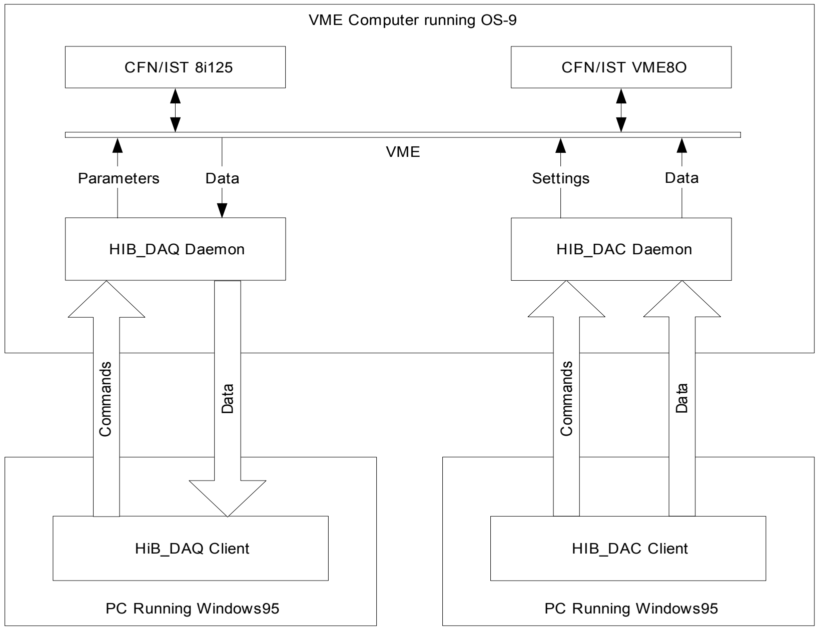

Figure 5.5 – Block diagram of the HIBD server/client architecture

when the magnetic well is reduced. The greatest rise in the level of fluctuations occurs when reducing the well from 2.4 to 0.9% suggesting an instability threshold somewhere in-between those two levels.

It has been observed that the decrease on the potential well introduces, apart from the increase on the fluctuation level, an increase on the radial and poloidal correlations (Figure 5.6). It seems that the stabilization effect of the magnetic well is due in part to an effective de-correlation of the fluctuations. The high values observed in the poloidal correlation are due, as previously seen in JET, to the poloidal velocity on the observation region.

Large-scale events propagate with faster velocities. The expected value of the effective velocity for a given radial correlation was computed at different magnetic wells (Figure 5.7). Although limited to the frequencies below 10 kHz (due to the used time window) an increase on the effective velocity is observed for events more radial correlated and this velocity increase with the decrease on the magnetic well. Results are consistent with the concept of transport self-regulated through ExB flows driven by fluctuations near marginal stability.

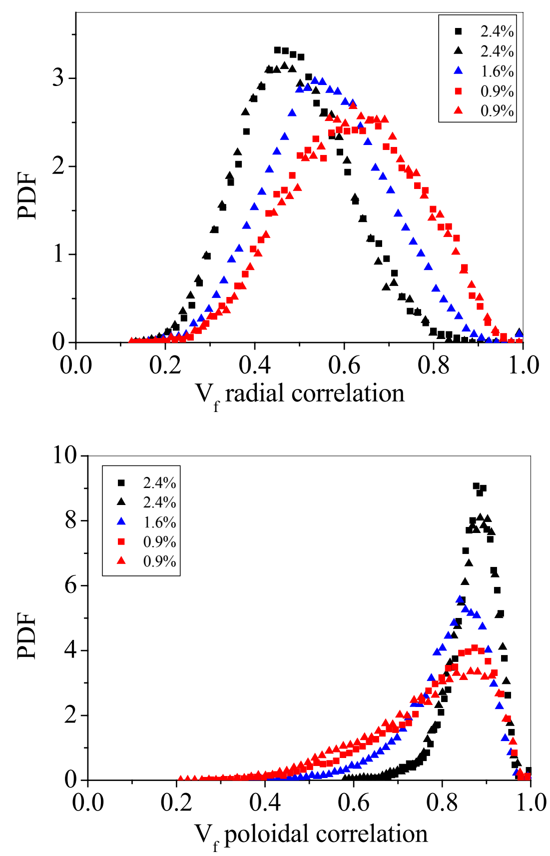

Figure 5.6 - PDFs of radial (a) and poloidal (b) correlations on floating potential fluctuations in TJ-II plasmas varying the magnetic well (0.9 – 2.4 %).

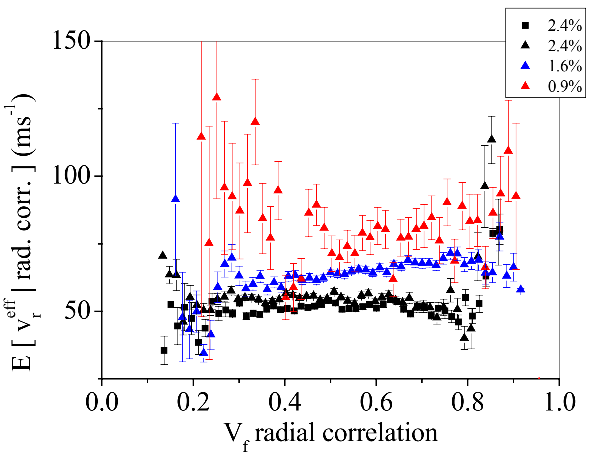

Figure 5.7 - Radial effective velocity versus radial correlation on the floating potential fluctuations in the TJ-II boundary region with different magnetic wells.